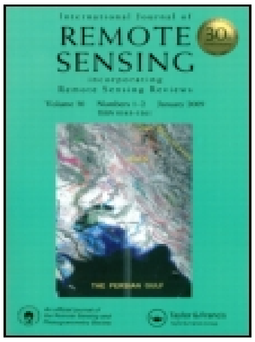

International Journal of Remote Sensing

ISSN: 0143-1161 (Print) 1366-5901 (Online) Journal homepage: http://www.tandfonline.com/loi/tres20

Derivation and validation of the seasonal thermal structure of Lake Malawi using multi-satellite AVHRR observations

M. Wooster , G. Patterson , R. Loftie & C. Sear

INT. J. REMOTE SENSING, 2001, VOL. 22, NO. 15, 2953–2972

Derivation and validation of the seasonal thermal structure of Lake Malawi using multi-satellite AVHRR observations

M. WOOSTER

Department of Geography, King's College London, Strand, London, WC2R 2LS, England, UK
e-mail: martin.wooster@ kcl.ac.uk

G. PATTERSON, R. LOFTIE and C. SEAR

The Natural Resources Institute, University of Greenwich, Chatham Maritime, Chatham, Kent, ME4 4TB, England, UK

(*Received 19 October 1999; in final form 15 May 2000*)

Abstract. Lake Malawi is the second largest lake in Africa by volume and an important regional source of food. Seasonal fluctuations in the primary production of the lake are principally controlled by the lake's thermal structure, which modulates the mixing of nutrient-rich deep water with that of the phytoplankton-rich near-surface layer. Satellites potentially offer an efficient, low cost method of providing information on the lakes thermal structure over the longer term via remote sensing observations of lake surface temperature. Here we investigate the accuracy of remotely sensed lake surface temperatures derived using data from the NOAA-11 AVHRR over a two-year period (1992–1993). Optimised triple window atmospheric correction algorithms are shown to provide an accuracy of around 0.5°C when compared to *in situ* water temperatures. The effect of the 1994 switch in operational night-time satellite from NOAA-11 to NOAA-14 is assessed using modelling of the transfer of radiation through the Malawian atmosphere, combined with detail on the differences in the satellite spectral response functions. These simulations indicate that lake surface temperatures derived from NOAA-14 are warmer than those that would be derived from NOAA-11 under the same conditions. The magnitude of the temperature difference is estimated at $0.27° \pm 0.07°C$, depending on the viewing zenith angle. Finally, we illustrate the ability of the remotely derived surface temperature maps to provide information relevant to the lakes 3-D thermal structure. Evaluations of the annual mixing regime of the lake can be based on this information, this mixing being directly relevant to the seasonal variations in lake primary production.

1. Introduction

Lake Malawi lies in the western arm of the East African Rift valley (figure 1) and is the second largest lake in Africa by volume, containing almost 7% of the Earth's liquid freshwater. There is strong vertical stratification in terms of temperature and nutrients, with nutrients depleted in the upper trophogenic region of the water column (Eccles 1974, Patterson and Kachinjika 1995). When the epilimnion temperature approaches that of the metalimnion (22.7–23.5°C) increased mixing occurs and nutrients are supplied to the trophogenic zone, with a resultant increase

International Journal of Remote Sensing
ISSN 0143-1161 print/ISSN 1366-5901 online © 2001 Taylor & Francis Ltd
http://www.tandf.co.uk/journals
DOI: 10.1080/01431160010006999

in phytoplankton productivity since this production is normally nutrient limited (Dengbol and Mapila 1982, Patterson and Kachinjika 1995). A similar increase in trophogenic zone nutrients is also the expected result of any large-scale upwelling of lake water, and the resulting increases in phytoplankton productivity have been shown to correlate with the productivity and survivability of the lake's pelagic fish community (Allison *et al.* 1995).

Because vertical mixing of the water column is so important to productivity, any study of the lake's large-scale primary production requires data on the 3-D thermal structure of the water and it's seasonal variation. Such data are normally obtained by interpolating vertical temperature profiles made during a series of lake transects. However, due to the size of Lake Malawi, this is a major and very costly undertaking that may take up to two weeks from a synoptic cruise to produce data for a single 3-D model. Interpretation of the data derived from such *in situ* sampling is also limited by difficulties in separating the effects of spatial and temporal water temperature variations, which may be highly significant within each sampling period. Satellite remote sensing provides a method of addressing these difficulties since a single overpass by a US National Oceanic and Atmospheric Administration (NOAA) polar orbiting satellite will provide Advanced Very High Resolution Radiometer (AVHRR) data of the entire lake surface (cloud cover permitting). These data can be used to map the lake surface brightness temperature variation using data from the AVHRR's three thermal infrared channels (3.7, 11 and 12 μm) at a spatial resolution of approximately 1.1 km^2 near nadir. Using variations of the atmospheric correction techniques commonly used to map the surface temperature distribution of the open ocean (e.g. McClain 1989) these brightness temperatures can theoretically be related to the true temperature of the lake's surface water. However, there are a number of uncertainties that remain to be addressed: (*i*) how precisely can the AVHRR brightness temperatures be related to the thermodynamic temperature of the surface epilimnion layer over the range of an annual cycle?; (*ii*) how is the accuracy of the temperature estimates affected by the changes in operational NOAA satellite that occur during long-term monitoring campaigns?; and (*iii*) how do the derived surface temperatures relate to the lake's 3-D thermal structure? The purpose of this paper is to address these questions by (*i*) calibrating and validating a long-term set of AVHRR-derived infrared brightness temperatures against a set of contemporaneous *in situ* epilimnion temperatures for Lake Malawi, (*ii*) using radiative transfer modelling to evaluate the effect of differing AVHRR thermal channel filter functions on the infrared brightness temperature measurements made under local conditions, and (*iii*) comparing maps of remotely-sensed lake surface temperature to contemporaneous data on the lake's three-dimensional thermal structure.

2. Remote estimation of surface water temperature using AVHRR

The remote estimation of sea surface temperature (SST) is a well developed operational application of AVHRR (Kidwell 1995, McClain 1989). The method generally involves combining infrared brightness temperature measurements from two or three of the AVHRR thermal channels in order to correct for the absorbing and emitting effects of the atmosphere, the so-called 'split-' and 'triple-window' atmospheric correction approaches first suggested by Anding and Kauth (1970). Optimisation of the algorithm coefficients can provide remote temperature estimates with a root mean square deviation (RMSD) of around 0.5°C from those taken by *in situ* floating buoys on the open ocean (Kidwell 1995). These methods should also be applicable to large inland lakes, with some uncertainty regarding the measurement precision due to potential differences between the atmosphere over lakes and that over open oceans. Such differences include the fact that (*i*) the atmosphere over inland lakes may not be in thermodynamic equilibrium with the water surface due to the effect of the warmer (daytime) or cooler (night-time) surrounding land, (*ii*) inland atmospheres may contain markedly increased concentrations of tropospheric aerosols compared to those over open oceans, and (*iii*) atmospheric thickness will vary depending on the altitude of the lake surface. These effects are likely to be most significant in tropical regions and may significantly effect the performance of AVHRR-based lake surface temperature algorithms. Derivation and testing of new split and triple window atmospheric correction algorithms for Lake Malawi allows the accuracy and precision of these optimised remotely sensed temperature measurements to be determined.

3. Application to Lake Malawi: algorithm derivation and accuracy assessment

3.1. *Daytime versus night-time data*

Disregarding viewing geometry variations, the AVHRR on each operational NOAA satellite observes a particular Earth location twice daily, with overpasses separated by approximately 12 hours (Kidwell 1995). For the period of the initial algorithm derivation and testing, commencing in 1992, the NOAA-11 satellite was the operational system. The satellite orbit meant the AVHRR imaged Lake Malawi within ± 1 hour of 01:30 (night-time) and 13:30 (daytime) local time each day. Hence it was first necessary to consider which overpass was the most appropriate for providing accurate data relevant to lake surface temperature.

Intensively sampled vertical profiles of epilimnion temperature were collected at the Nkhata Bay station (11°36′S, 34°30′E) (figure 1). These were made using a purpose-built continuous temperature/depth probe (Plymouth Marine Laboratory, UK). Figure 2 shows a depth/time plot of a 24 hour study on 6 and 7 April 1992 at this station. Isotherms were plotted using the *Surfer* software package (Golden Software Inc.).

It is clear that after around 10:00 h local time, absorption of solar radiation by the upper water column results in the formation of a diurnal thermocline. The thermocline strength peaks around 14:00 h, which is close to the 13:30 h daytime overpass time of NOAA-11. This indicates that lake surface temperatures retrieved from daytime satellite imagery are representative of only the top few meters of the water column. The magnitude of the diurnal thermocline effect would be expected to increase still further during the hottest months (October–December), especially during periods of low wind speed. In contrast the night-time satellite overpass around 01:30 h occurs when water temperatures at the near surface (1 m depth) are representative of the bulk mixed layer, in the case of figure 2 being within 0.1°C of those at 25 m depth. This is confirmed by profiles made on other dates and, since the mixing of epilimnion and metalimnion waters is dependent upon the temperature of the bulk epilimnion layer, these data suggest that the night-time overpass of the NOAA-11 satellite is most appropriate for hydrodynamic investigations.

An insight into the spatial variation of the diurnal thermocline can be gained from direct comparison of AVHRR geocoded daytime and night-time imagery (figure 3). These data were processed using the split window algorithm of McClain *et al.* (1985), which was found to give the best performance on Lake Malawi during the pilot study of Wooster *et al.* (1994a). A mean surface temperature difference of

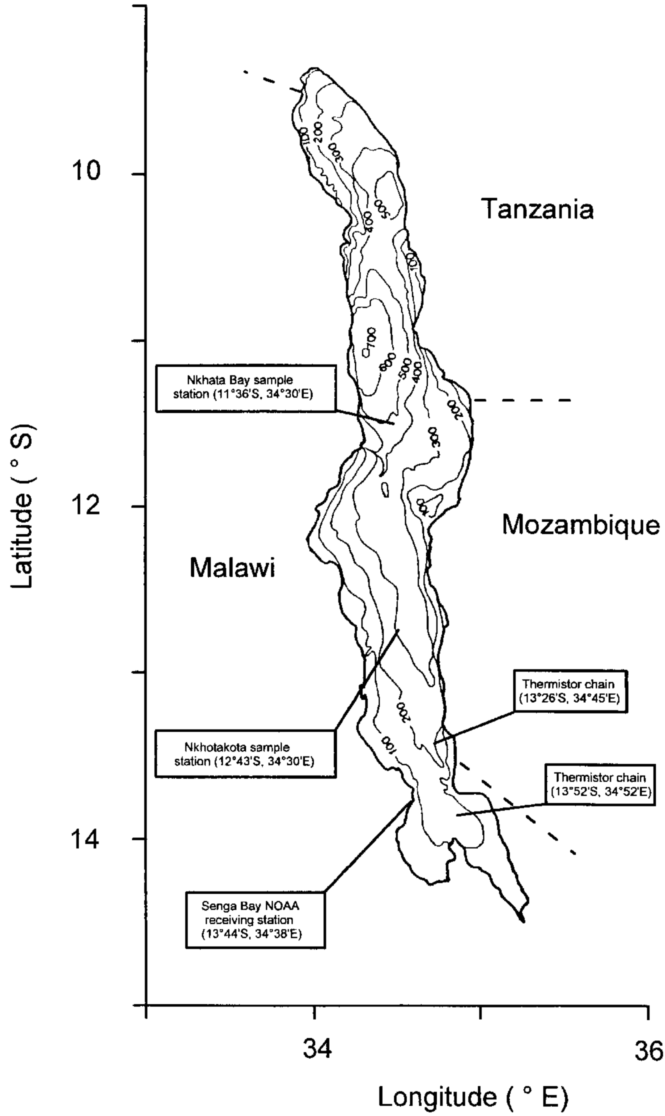

Figure 1. Lake Malawi showing the location of the Nkhata Bay and Nkhotakota sampling stations and the Senga Bay NOAA receiving station.

0.75°C is observed between daytime and night-time conditions, but there is a high degree of spatial variation with a maximum temperature difference of 3°C. A proportion of this variation will be due to fluctuations in the surface skin effect (Hepplewhite 1989), but the majority is likely to be due to spatial variations in the magnitude of the diurnal thermocline, as described above.

3.2. *New algorithm derivation: split versus triple window*

For routine collection of NOAA-11 night-time data, a PC-based NOAA AVHRR High Resolution Picture Transmission (HRPT) receiving station was installed at the lake-shore research station at Senga Bay, Malawi (Wooster *et al.* 1994b). After HRPT

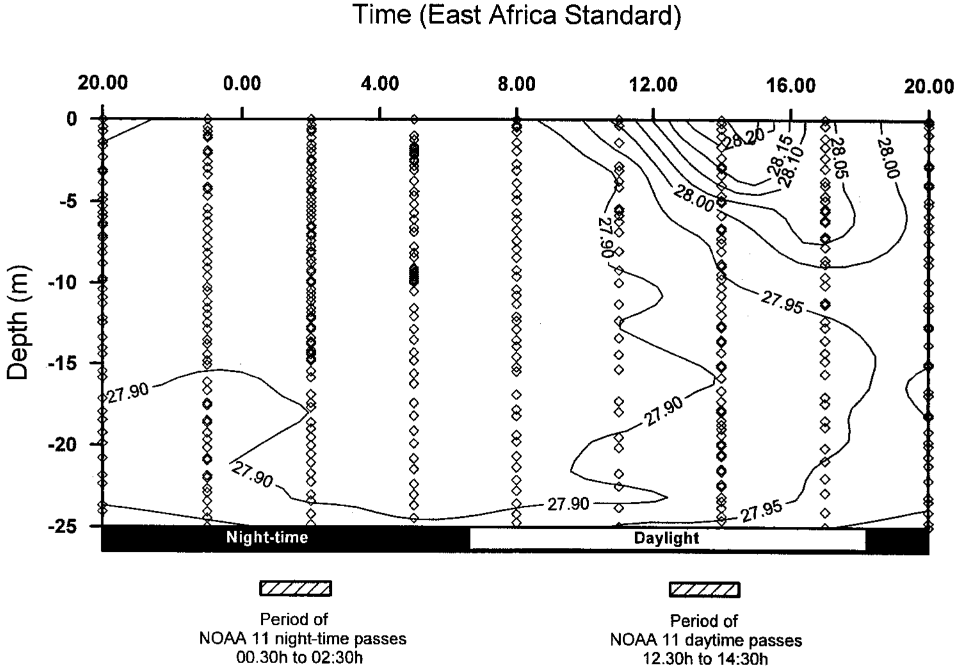

Figure 2. Contour plot showing the relationship between water temperature, depth and time at the Nkhata Bay sampling site on 6–7 April 1992. The daylight period for 7 April 1992 is indicated, as well as the overpass times of the NOAA-11 satellite during the period of the study (1992–1994). Diamond symbols indicate the location of each temperature measurement. Local time in Malawi is East Africa Standard, equivalent to GMT+2 hours.

data capture, the AVHRR data are extracted and converted into geocoded maps of lake surface brightness temperature in the three AVHRR thermal channels, using the calibration techniques detailed in Wooster *et al.* (1995). Detection of cloud contaminated pixels was based on the multi-channel brightness temperature comparison techniques of Saunders and Kriebel (1988), with threshold alterations made to account for the tropical atmosphere. During an initial eight month period in 1992 *in situ* surface temperature data were collected from the roving research vessel, R/V *Usipa*. These night-time measurements were made every hour between 21:00 h and 06:00 h, and gave a wide coverage of lake surface temperature as they followed the cruise pattern laid down by the fish acoustic survey (Menz *et al.* 1995). Water was sampled using a *Khalsico* thermometer bucket with a mercury stem thermometer accurate to ± 0.1°C. Using these data Wooster *et al.* (1994a) made a preliminary test of the applicability of published SST algorithms for the remote measurement of tropical lake surface temperature. Though this limited data set did not cover full seasonal range, results suggested that an accuracy similar to that obtained over the open ocean could be expected with suitably optimised algorithms. A significantly expanded satellite and *in situ* data set covering a full two year period (1992–1993) has now been compiled for the optimisation and testing of new algorithm coefficients. The complete data set consists of 65 data pairs of cloud-free AVHRR pixels and corresponding *in situ* water temperature measurements taken either during the same night or on immediately neighbouring nights. This temporal limit was calculated from analysis of the maximum change in near surface (1 m) temperature, based on data from the second fixed station (the Nkhotakota station 12°43′S, 34°30′E; figure 1). This station was visited a total of 29 times in 1992 and 1993 to produce a seasonal depth-time plot (Patterson and Kachinjika 1995). From this a maximum rate of change of 0.15°C day^{-1} was demonstrated. Half (33) of the data pairs were randomly selected as Matchup Set A and used to empirically derive new algorithm coefficients optimised for local conditions (equations 1 and 2). The techniques used for algorithm derivation were the regression-based procedures outlined in Wooster *et al.* (1994b), with the relative strength of the satellite versus *in situ* data relationship indicated by the correlation coefficient and RMSD values resulting from the derivation procedure.

Split Window ($r^2 = 0.34$, RMSD = 0.69°C)

$$\mathrm{LST} = 2.1226\,T_4 - 1.1226\,T_5 - 271.16 \tag{1}$$

Triple Window ($r^2 = 0.92$, RMSD = 0.39°C)

$$\mathrm{LST} = 0.9115\,T_3 + 0.9191\,T_4 - 0.8246\,T_5 - 273.21 \tag{2}$$

where LST is lake surface temperature (°C), T_3 is the AVHRR channel 3 (3.7 μm) brightness temperature (K), T_4 is the AVHRR channel 4 (11 μm) brightness temperature (K), T_5 is the AVHRR channel 5 (12 μm) brightness temperature (K).

The most appropriate and robust test of the accuracy and precision of these new equations was to evaluate their performance when applied to an independent satellite and *in situ* dataset. For this purpose we utilised the remaining 32 data pairs (Matchup Set B) not used in the algorithm derivation procedure, with results shown in figure 4. With this independent dataset the scatter exhibited by the triple window algorithm is much reduced in comparison to the split window algorithm, with a consequent reduction in the overall measure of root mean square deviation between the *in situ* and satellite-based measurements. The superior performance of the triple window technique agrees with the pilot study results using previously published split and triple window SST algorithms (Wooster *et al.* 1994a).

The reason for the effectiveness of including AVHRR channel 3 measurements in the surface temperature derivation can be investigated by comparing the brightness temperature differences between the various AVHRR thermal channels to a measure of the overall atmospheric effect on the signal. In this case the atmospheric effect is represented by the deficit between the actual *in situ* temperature measurement and the brightness temperature recorded in AVHRR channel 4. Figure 5(*a*) shows that the brightness temperature difference between AVHRR channels 4 and 5 is well correlated to the magnitude of the atmospheric effect. This relationship results from the fact that AVHRR channels 4 and 5 split the 8–14 μm atmospheric window and are thus differentially sensitive to water vapour absorption. This is the basis of the split window atmospheric correction method originally proposed by Anding

Figure 3. The difference in lake surface temperatures retrieved using NOAA-11 AVHRR data collected at 15:18 h on 26 August 1992 and 02:28 h on 27 August 1992 (all times are local). The mean temperature difference is 0.75 ± 0.61°C (analysis of 24 932 cloud free pixels). Bulk water temperatures are not expected to have altered significantly in the 11 hour period between satellite overpasses, thus the observed temperature difference is predominantly due to the formation of a daytime diurnal thermocline.

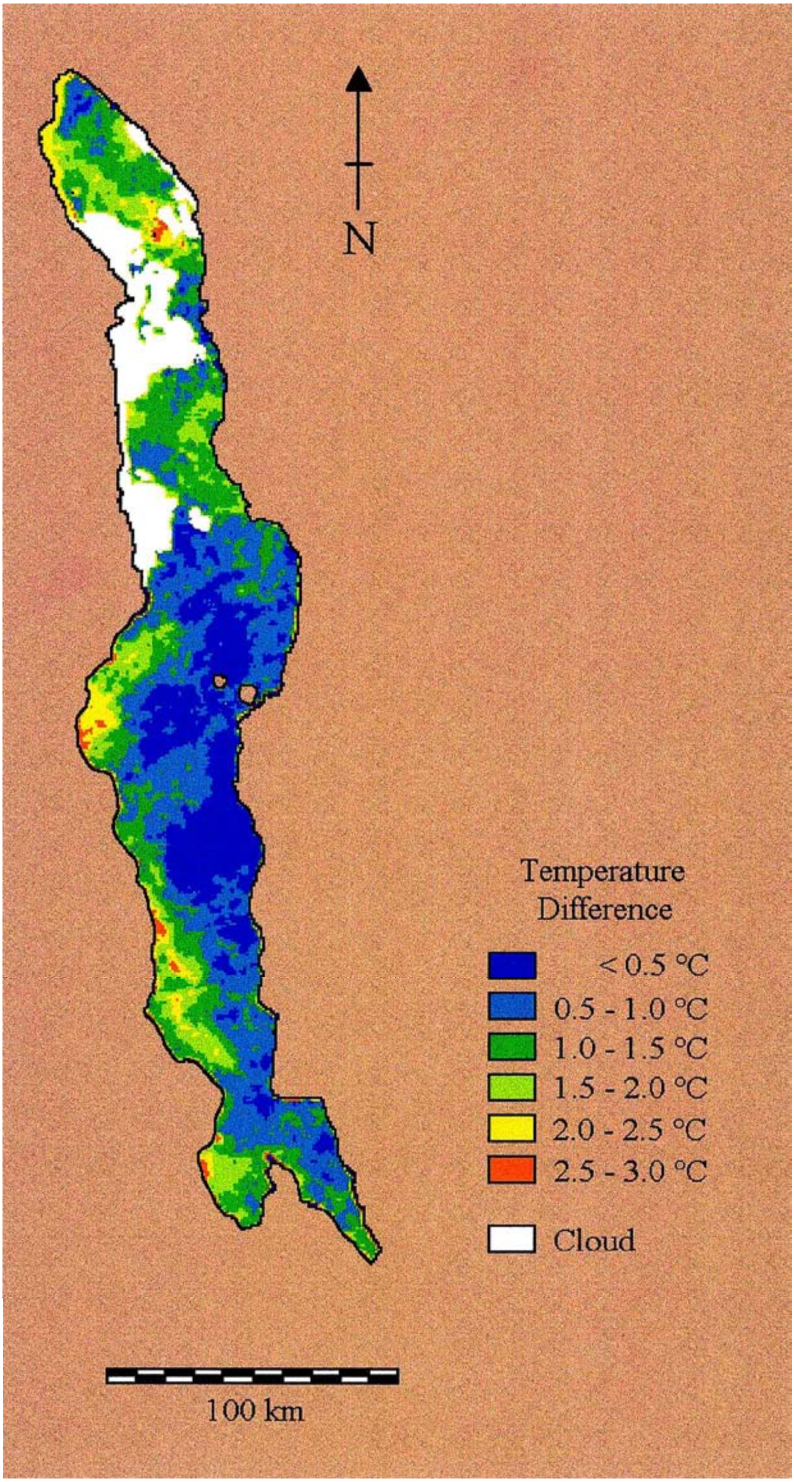
N
Temperature Difference
< 0.5 °C
0.5 - 1.0 °C
1.0 - 1.5 °C
1.5 - 2.0 °C
2.0 - 2.5 °C
2.5 - 3.0 °C
Cloud
100 km

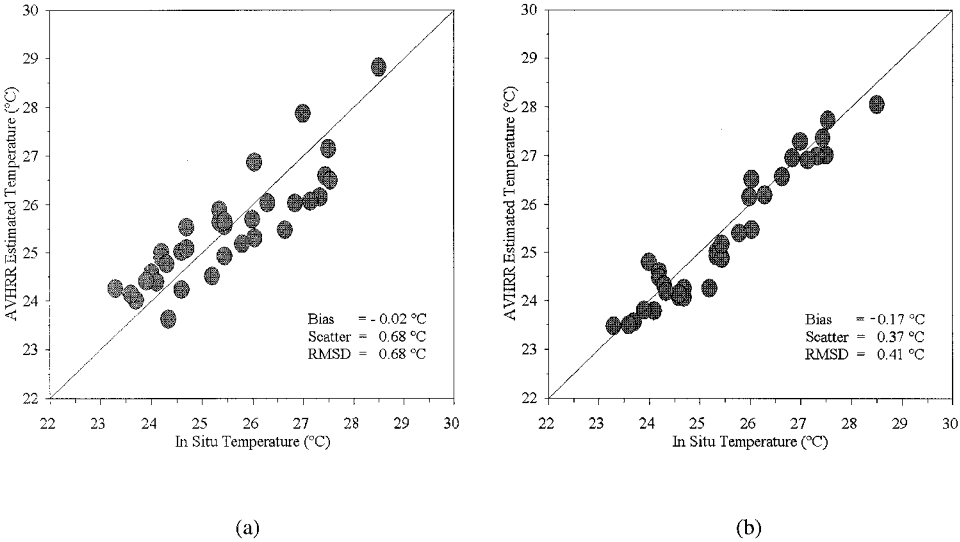

Figure 4. The new (*a*) split window, and (*b*) triple window algorithms, derived with Matchup Set A and tested with Matchup Set B.

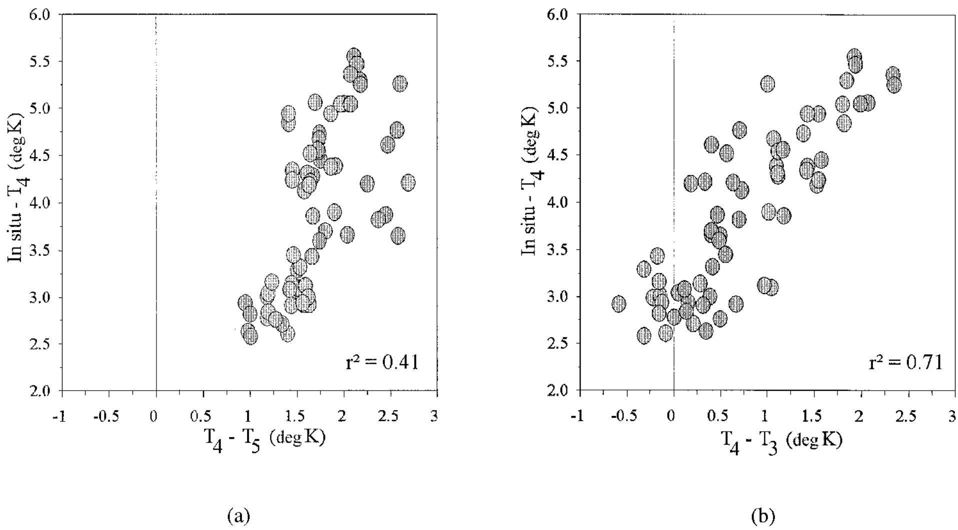

Figure 5. The relationship between the brightness temperatures measured in the AVHRR thermal channels and the magnitude of the atmospheric effect, represented by the temperature deficit between the *in situ* temperature measurement and the AVHRR channel 4 brightness temperature. Data are derived from the 65 matchup points used in the current study. The magnitude of the atmospheric effect is significantly correlated to the channel 4–5 brightness temperature difference (figure 5(*a*)), but a stronger correlation is observed with the channel 3–4 brightness temperature difference (figure 5(*b*)). This highlights the importance of using AVHRR channel 3 measurements in the tropical atmospheric correction algorithm.

and Kauth (1970). However, figure 5(*b*) indicates the relationship is significantly strengthened by replacing the brightness temperature difference between AVHRR channels 4 and 5 with that between channels 3 and 4. This is because measurements made in AVHRR channel 3 are less affected by atmospheric water vapour than are those made at the longer wavelengths of channels 4 and 5 (Hepplewhite 1989). Thus for high humidity atmospheres the AVHRR channel 3–4 brightness temperature difference will provide a stronger measure of the atmospheric effect than will the brightness temperature difference recorded in the so-called split window channels. The tropical nature of the Malawian atmosphere thus necessitates the use of AVHRR channel 3 data if the performance of the atmospheric correction procedure is to be maximised. This result also illustrates a further advantage of using night-time AVHRR data, since reflection of solar radiation from the water surface prevents quantitative use of daytime 3.7 μm observations.

3.3. *Use of angularly varying coefficients*

In addition to incorporating data from AVHRR channel 3, a further method of algorithm optimisation is to vary the algorithm coefficients in proportion to the air mass between the satellite and ground pixel (Llewellyn-Jones *et al.* 1984, Barton *et al.* 1989). The air mass is dependent upon the viewing zenith angle, which in the case of AVHRR data captured in Malawi was limited to a maximum of 50° in order to avoid near-horizon satellite overpasses. To gauge the effect of varying view angle on the retrieved estimates of lake surface temperature, the difference between the *in situ* and AVHRR-derived lake surface temperatures was plotted as a function of viewing zenith angle (figure 6). No consistent relationship is apparent, though the location with the highest air mass also exhibits the largest temperature difference.

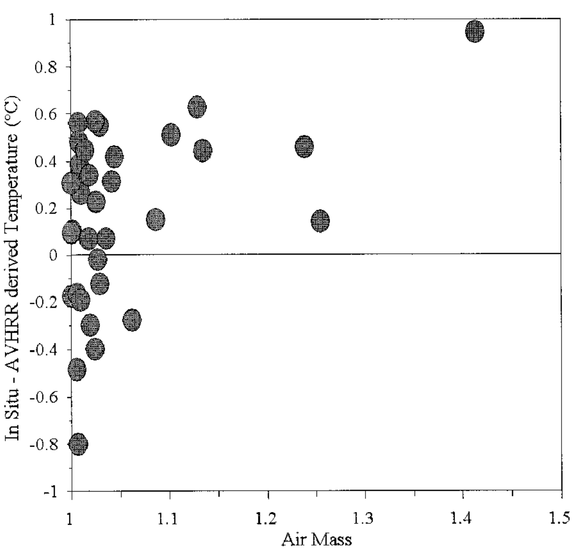

Figure 6. The difference between the *in situ* and AVHRR-derived lake surface temperatures, as a function of the air mass between the satellite and the matchup location. The AVHRR LST measurement was made using equation (2) and air mass = sec(viewing zenith angle).

A new triple window algorithm which incorporated angularly varying coefficients was derived using Matchup Set A.

$$\text{Angularly varying triple window } (r^2 = 0.94,\ \text{RMSD} = 0.36^\circ\text{C})$$

$$\begin{aligned}\text{LST} = {} & (1.0650 - 3.6803A)T_3 + (0.7523 + 2.986A)T_4 \\ & - (0.7955 - 0.7090A)T_5 - 277.98 \end{aligned} \tag{3}$$

Where $A = \text{airmass} - 1 = \sec(\text{viewing zenith angle}) - 1$.

Accuracy assessment was again carried out using the independent Matchup data set B. An RMSD of 0.36°C was obtained, which is a small (0.05°C) improvement on that obtained with non-angularly dependent coefficients (equation 2). This is insignificant compared to overall algorithm accuracy and, given the viewing geometry limits set by the data capture system, equation (2) was chosen as most appropriate for routine LST derivation.

3.4. *Aerosol effects*

Under most atmospheric conditions, the AVHRR brightness temperatures retrieved for the lake surface will decrease with increasing thermal channel wavelength due to the increasing effectiveness of atmospheric water vapour absorption over this region of the electromagnetic spectrum (Llewellyn-Jones *et al.* 1984). However, as figure 5(*b*) illustrates, the retrieved brightness temperatures are sometimes lower in AVHRR channel 3 than in channel 4. This could potentially result from the effect of a strong atmospheric temperature inversion, but in this case the normal channels 4 and 5 brightness temperature relationship would also be reversed (i.e. $T_5 > T_4$), which is not observed. We therefore suggest that a more likely explanation is the interaction of the surface emitted radiation with atmospheric aerosols, particularly dust particles and haze from vegetation fires. Hepplewhite (1989) shows that brightness temperature deficits due to atmospheric aerosols are many times more significant for AVHRR channel 3 than for the longer channel 4 or 5 wavelengths. Furthermore, we only observed depressed channel 3 brightness temperatures at the end of the 1992 and 1993 dry seasons, the period when concentrations of atmospheric dust and haze is maximised. However, since these anomalous observations were not the ones to exhibit the largest differences between the *in situ* and AVHRR-derived LST's, the effects of this phenomenon are believed to be relatively minor. Further research to investigate the potential advantage of deriving aerosol resistant algorithms (e.g. Walton 1985) would most likely be beneficial.

3.5. *Changes in the operational NOAA satellite*

The onboard calibration system for the AVHRR thermal channels allows in-orbit sensor variations to be compensated for during routine data processing (Kidwell 1995). However, since there are differences in the spectral response functions of corresponding thermal channels on different AVHRR instruments, there maybe residual effects when switching between data obtained from different satellites (Kidwell 1995). The Lake Malawi triple window atmospheric correction algorithm (equation 2) was derived from empirical analysis of NOAA-11 AVHRR data. In 1994 the NOAA-11 AVHRR failed on 13 September and in December the NOAA-14 satellite was launched as a replacement. An investigation into the effect of this satellite change on the accuracy and precision of equation (2) was required if long-term monitoring of the lake was to be continued using NOAA-14.

The spectral response functions for the AVHRR instruments on the NOAA-11 and NOAA-14 satellites are shown in figure 7. In general the NOAA-14 AVHRR channels are shifted to slightly longer wavelengths than the corresponding channels of NOAA-11. Figure 7 also illustrates that the atmospheric effect on the water-leaving thermal radiance, illustrated here by the atmospheric transmission, also varies considerably across the wavebands. The combination of the inter-satellite spectral response variations and the wavelength varying atmospheric effect will cause the corresponding channels of the two AVHRR instruments to measure slightly different brightness temperatures for the same emitting temperature of the water surface. Since equation (2) combines a series of multi-channel brightness temperatures, the lake

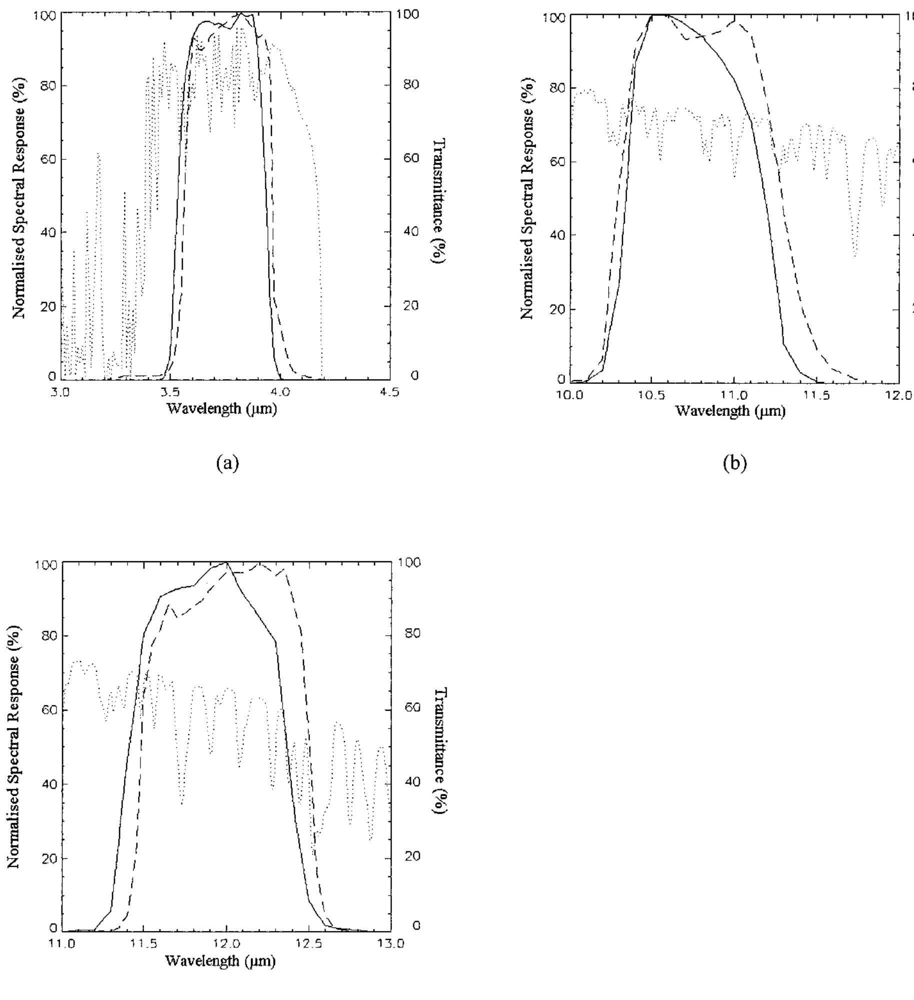

Figure 7. The normalised spectral response functions of the NOAA-11 (solid) and NOAA-14 (dashed) AVHRR thermal channels centred around (*a*) 3.7 μm, (*b*) 11 μm, and (*c*) 12 μm. These data are taken from Kidwell (1995). Also plotted on the right hand side *y*-axis is the atmospheric transmission over these wavebands (dotted line) for the Lake Malawi atmosphere sampled on 14 November 1992, calculated using the MODTRAN radiative transfer model.

surface temperature output may differ significantly when using data from the two different AVHRR instruments. Unfortunately a direct comparison of contemporaneous NOAA-11 and NOAA-14 AVHRR data was not possible since the satellites did not operate simultaneously. Nor were high precision *in situ* temperature data available for comparison with NOAA-14 imagery since, after the derivation and testing of equation (2), routine monitoring of the lake temperature is conducted using remote sensing methods only. Instead the magnitude of the NOAA 11 to NOAA 14 switch was gauged using simulated NOAA-11 and NOAA-14 brightness temperature measurements, constructed using a radiative transfer code parameterised with data of the Malawian atmosphere. Using these simulated measurements in equation (2), it is possible to predict the differences in remotely sensed lake temperature that would be obtained by the two satellites when observing the lake under identical viewing conditions.

The MODTRAN radiative transfer code (Berk *et al*., 1989) was parameterised with historical atmospheric profile data taken by the Malawi Meteorological Department in Lilongwe during March, September and December 1977. Using the techniques of Byrnes and Schott (1986) the lower section of these profiles were adjusted to represent conditions over the lake surface using contemporaneous data from the lake-shore meteorological station at Salima. These historical data were also supplemented with data from two more recent radiosonde ascents, collected directly over the lake in November 1992 (Brown 1995). The MODTRAN code was parameterised with each atmospheric profile in turn and used to simulate the path of thermal radiation from the lake surface to the satellite and to predict the top-of-atmosphere (TOA) spectral radiance over the entire wavelength range covered by the AVHRR thermal channels shown in figure 7. For each profile the emitting surface water temperature was varied in 2°C intervals between 20°C and 30°C, encompassing the full range of lake surface temperatures, and the viewing zenith angle was varied between 0° and 50°. The spectrally varying fresh water emissivities given by Masuda *et al*. (1988) were assumed. The TOA radiance data resulting from each model run were convolved with each AVHRR channel spectral response function to provide a prediction of the measured spectral radiance over each AVHRR waveband. Following the description of Cracknell (1997), the corresponding AVHRR channel brightness temperatures were then calculated using iteration of equation (4), given in the NESS107 supplement to Kidwell (1995), until the assumed brightness temperature value reproduced the calculated channel spectral radiance.

$$\text{Spectral Radiance } (\mathrm{Wm^{-2}\,sr^{-1}\,\mu m^{-1}}) = \frac{\sum_{i=1}^{n} B(\lambda_i, T)\Delta\lambda R_i(\lambda_i)}{\Delta\lambda R_i(\lambda_i)} \tag{4}$$

where T is the channel brightness temperature, B is the Plank Function spectral radiance ($\mathrm{Wm^{-2}\,sr^{-1}\,\mu m^{-1}}$), n is the number of measurements comprising the channel spectral response function, $\Delta\lambda$ is the wavelength increment between the measurements of spectral response (μm), R_i is the normalised spectral response function at location i (unitless) λ_i is the wavelength at spectral response function location i (μm)

The calculated channel brightness temperatures were then used within equation (2) to reproduce the lake surface temperatures that would be obtained by the two satellite instruments when observing the lake under the same viewing conditions.

As an example figure 8 shows the radiosonde profile data taken on 14 November, 1992, and figure 9 shows the difference in the NOAA-11 and NOAA14 derived lake surface temperature estimates, calculated using these radiosonde data within the MODTRAN code and simulating observations at the two stated viewing conditions and six surface temperatures. These data indicate that there is a difference in the

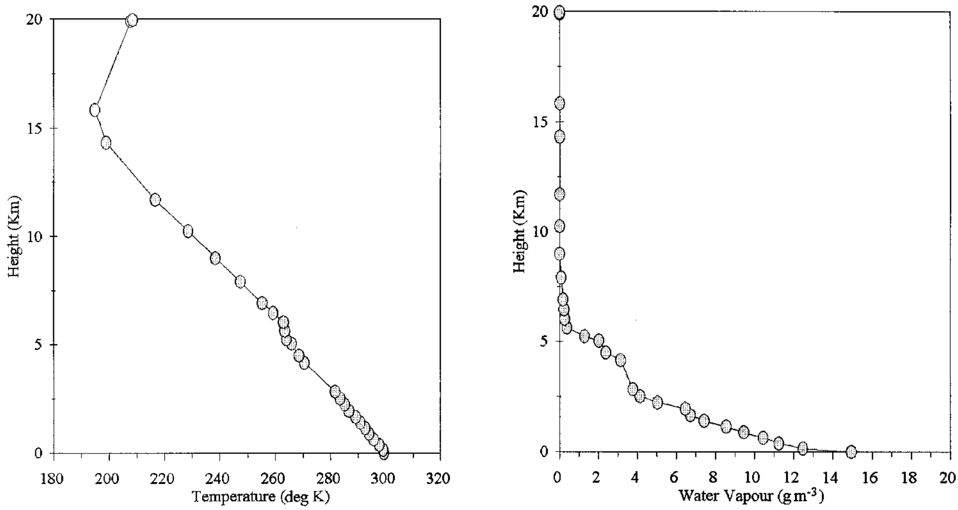

Figure 8. The temperature and water vapour profile of the atmosphere over Lake Malawi, sampled by radiosonde on 14 November 1992.

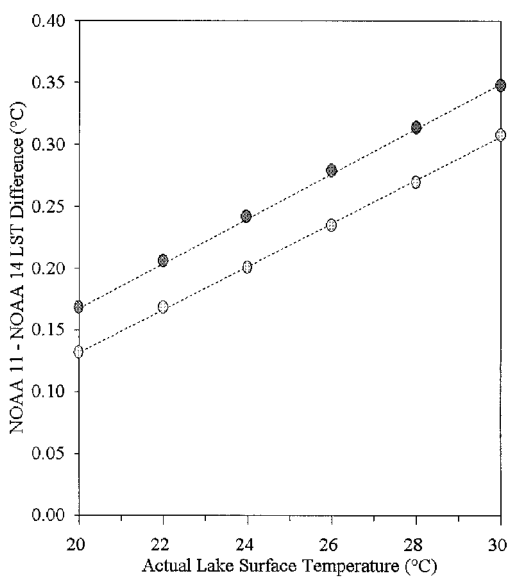

Figure 9. The difference in the estimates of lake surface temperature (LST) calculated using simulated NOAA-14 and NOAA-11 AVHRR brightness temperatures within equation (2) for nadir (lower line) and far off-nadir (upper line) conditions. Brightness temperature values were simulated using the radiosonde data of figure 8 within the MODTRAN code, with zenith angle $=0°$ for nadir, and zenith angle $=50°$ for far-off nadir observations. Dotted lines indicate the best linear fit to each set of data points.

lake surface temperatures calculated using the NOAA-11 and NOAA-14 AVHRR instruments under these atmospheric conditions, and that this difference increases with the surface temperature of the lake and with the zenith angle used to make the observation. However, the data indicate that the magnitude of the effect is relatively small, with values of 0.21 ± 0.8°C for the nadir observations, and 0.25 ± 0.8°C for the far off-nadir observations. Analysing the difference in the individual channel brightness temperatures indicates that the AVHRR channel 3 measurements are negligibly affected by the change in satellite, with a maximum brightness temperature difference of 0.02°C, whilst the AVHRR channel 5 measurements are most significantly affected, with a maximum brightness temperature difference of 0.6°C. This reflects both the varying nature of the spectral response function differences between channels shown in figure 7, and the fact that the atmospheric effect generally increases with increasing channel wavelength.

Figure 10 shows the lake surface temperatures retrieved from the NOAA-11 and NOAA-14 AVHRR simulations, using all sampled atmospheres and all simulated viewing conditions. It can be seen that the temperature estimates made using the two satellites are very highly correlated ($r^2 > 0.99$), with estimates made using simulated NOAA-14 AVHRR data 0.27 ± 0.07°C higher than the corresponding estimates made with simulated NOAA-11 AVHRR data. This positive bias will counteract the negative (−0.17°C) bias originally exhibited by equation (2) when tested with NOAA-11 AVHRR and *in situ* data (figure 4(*b*)). In this way it is predicted that a bias of only around 0.1°C should result between *in situ* LST measurements and the corresponding estimates produced from application of equation (2) to NOAA-14 AVHRR data. The magnitude of this predicted bias is lower than the noise level of the AVHRR sensor (Kidwell, 1995) and of the same order as the 0.1°C precision of the

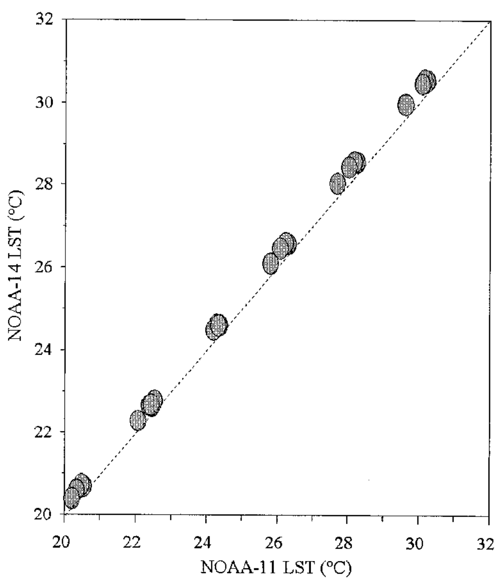

Figure 10. Modelled NOAA-14 and NOAA-11 lake surface temperature (LST) measurements for a range of actual surface temperature and view angle conditions. LST measurements were calculated using NOAA-11 and NOAA-14 AVHRR brightness temperatures simulated using the MODTRAN code with a seasonal range of Lake Malawi atmospheric profile data. The 1:1 line is indicated.

in situ measurements used in the original algorithm derivation and testing. As previously mentioned, due to the logistics involved in making extended high precision *in situ* temperature measurements from the research vessel, no long-term *in situ* data of a similar precision are available for direct comparison with temperature estimates provided by NOAA-14. However, for periods interspersed throughout 1997–98 night-time *in situ* temperatures are available from two thermistors/data loggers that were anchored at around 1 m depth at 13°26′S, 34°45′E and 13°52′S, 34°52′E (figure 1). Due to the differing methodology, the precision of these measurements is lower than the 0.1°C quoted for the original bucket temperature measurements, but they provide an empirical method of testing for any gross errors in the temperature estimates derived using equation (2) with NOAA-14 data. Matchups were made between these thermistor data and NOAA-14 AVHRR images taken within 1 hour of the thermistor measurement on twenty occasions in 1997–98, spaced approximately evenly throughout the less-cloudy May–November period. Two bucket temperature measurements made from the research vessel over this period were also matched to cloud free imagery. Figure 11 shows the results of this matchup study, with a positive bias of 0.06°C between the satellite and *in situ* data. This compares with the negative bias originally obtained when using NOAA-11 data (figure 4(*b*)) and helps confirm the suggestion that, viewed through the same atmosphere, water surface temperatures derived via NOAA-14 observations are slightly warmer than those derived via NOAA-11. The scatter of the data shown in figure 11 is a little higher than that obtained during original testing of the new triple window algorithm (figure 4(*b*)), which probably reflects the lower precision of the thermistor measurements compared to those made using the bucket measurement technique. Overall the results from the empirical study confirm the hypothesis developed using the radiative transfer

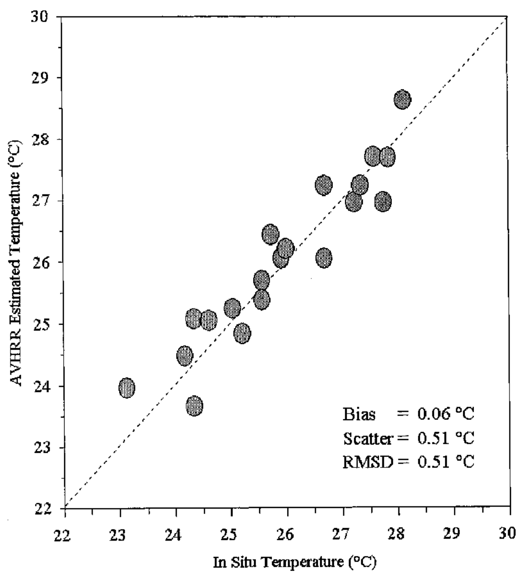

Figure 11. The matchup data set for empirical testing the accuracy of the NOAA-14-derived lake temperature estimates. The AVHRR estimated temperatures were derived using triple window equation (2) with NOAA-14 AVHRR data, whilst the *in situ* data set consists of thermistor and bucket temperature measurements made within one hour of the corresponding satellite overpass.

modelling, in that the NOAA-14 derived LST measurements possess a negligible temperature bias in comparison to the measurement precision. They indicate that when using NOAA-14 AVHRR data to estimate the surface temperature of the lake with equation (2), an RMSD accuracy is obtained that is comparable to that achieved using the NOAA-11 AVHRR data for which the algorithm was originally designed, i.e. around 0.05°C.

4. Seasonal monitoring of lake thermal structure

In order to validate their use in limnological and hydrological studies, the images of lake temperature retrieved using remote sensing must be compared to three-dimensional data on the lake water structure, derived using the standard methods of direct *in situ* sampling and data interpolation. For this purpose our *in situ* data consisted of vertical temperature profiles collected during a series of research cruises in 1992 and 1993. Temperature measurements were made using a hydrographic probe and were taken along the central north–south axis of the lake to around 320 m depth (or close to the bottom if shallower). Satellite-derived LST maps were produced from the application of equation (2) to night-time NOAA-11 AVHRR data acquired on a near-daily basis from May 1993 to September 1994. This period partly overlapped with the *in situ* cruise sampling period carried out between January 1992 and January 1994. Useful comparisons between these data sets were not possible for the mid- to late-wet season (January–March 1994) due to excessive cloud cover. However, this is the hottest period of the year and it was shown for previous years to be a period when thermal stratification of the lake water was strongest and thus mixing was at a minimum (Patterson and Kachinjika 1995). Outside of this period there is good agreement between all the *in situ* and satellite-derived datasets. Figure 12 shows a good example from July 1993, with the water temperature structure derived from interpolation of a series of lake-wide *in situ* temperature profiles compared to the AVHRR-derived lake surface temperature map of the same period. This LST map is derived from maximum value compositing of four separate July 1993 LST images, each of which had part of the lake obscured by cloud. A 3×3 smoothing algorithm was applied to reduce the effect of AVHRR sensor noise (Llewellyn-Jones *et al.* 1984) and the land has been masked using a GIS data file of the lake shoreline.

The major thermal feature in July 1993 (figure 12) is the presence of a significant cold water plume located around the position of the second vertical profile (midway across the lake at a latitude of around 10°11′S). On the profile data the plume is apparent at this location as a set of near vertical contours, with colder water apparently rising to the surface from the metalimnion layer at around 100 m depth. Such a vertically rising cold water plume is expected to have significantly increased the photic-zone nutrient concentration in this region of the lake. On the satellite-derived lake surface temperature map the plumes presence at the stated location is indicated by a colder patch of surface water of around 30 km^2, exhibiting temperatures around 1°C cooler (24.25–24.75°C, green on the LST map) than the immediate surrounding surface water (yellow-orange-red on the LST map). A few months after the July 1993 upwelling a similar cold water event was again noted on LST maps of the northern lake region, and Patterson *et al.* (1995) describe how these 1993 upwellings were correlated with higher levels of zooplankton and fish larvae production when compared to the latter part of 1992, when no such upwellings were noted. These comparisons confirm that real, large-scale limnological events having direct relevance to lake productivity are observable using the remote sensing technique.

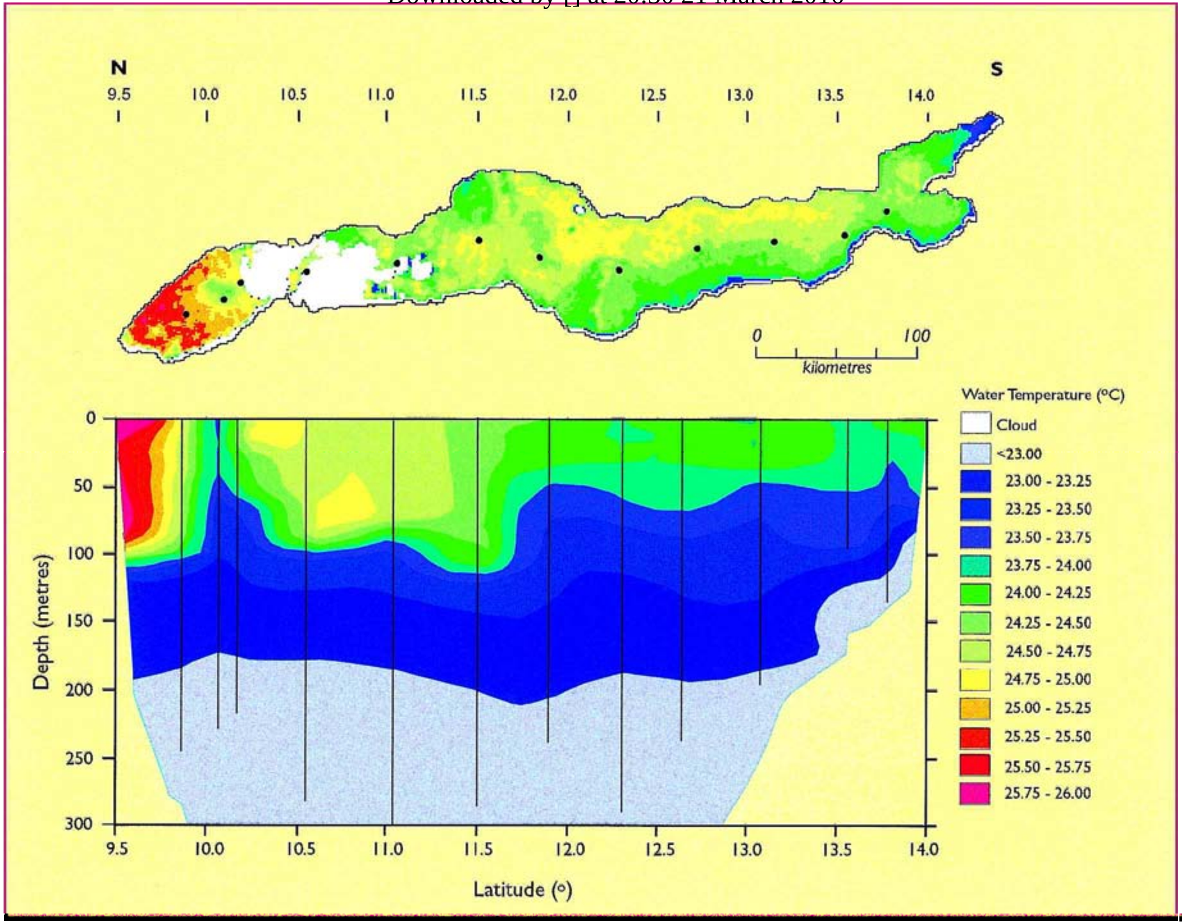

Figure 12. Lake surface temperature map derived from application of equation (2) to night-time NOAA-11 AVHRR data collected in July 1993, along with a depth-latitude plot of lake water temperature derived from research cruise data collected over the same period. The LST image is a composite of four separate datasets (11, 19, 20 and 22 July 1993) in order to minimise cloud cover, whilst the cruise data were collected between 13 and 22 July 1993. Vertical lines on the depth-latitude plot indicate the probe profiles used to construct the lake water isotherms, with the corresponding horizontal probe locations marked on the LST image.

Using the extended satellite time-series, the overall seasonal pattern of water temperature variation within the bulk epilimnion layer can be deduced. Figure 13 shows the mean and standard deviation of the whole lake surface temperature for the 17 month period of initial satellite data collection. Each point on the figure corresponds to a low cloud cover ($<10\%$) image of the lake and is calculated from all cloud-free lake pixels ($n > 20\,000$). The results indicate that mean lake epilimnion temperature reaches a minimum in August, when vertical mixing is assumed to be at a maximum. September 1993 and 1994 sees an upturn in mean lake epilimnion temperature, related to atmospheric warming and a reduction in evaporative cooling caused by reduced winds. Such near-continuous temperature data are useful for the calculation of water density and can be applied to the calculation of parameters (such as the Wedderburn number) which define the dominant tendency of a water body i.e. mixing or stratification (Talling and Lemoalle 1998). Patterson *et al.* (1995) indicate how Wedderburn numbers calculated using remote sensing data of this type for Lake Malawi can reliably reproduce those calculated from *in situ* measurements, thus allowing the mixing regime to be quantitatively assessed from remote sensing and meteorological data alone (assuming some knowledge of metalimnion density).

5. Conclusion

This study has indicated that night-time NOAA-11 AVHRR observations combining data from all three AVHRR thermal channels can provide estimates of the near-surface (1 m depth) water temperature of Lake Malawi to a RMSD accuracy of around 0.5°C when compared to *in situ* water temperature measurements. A new triple window atmospheric correction algorithm is presented for this purpose. The effect of the switch in operational night-time satellite from NOAA-11 to NOAA-14 at the end of 1994 has been assessed and it has been shown that accurate lake surface temperatures can continue to be derived from these new NOAA-14 data without the need for major algorithm alteration. Comparison with vertical temperature profiles

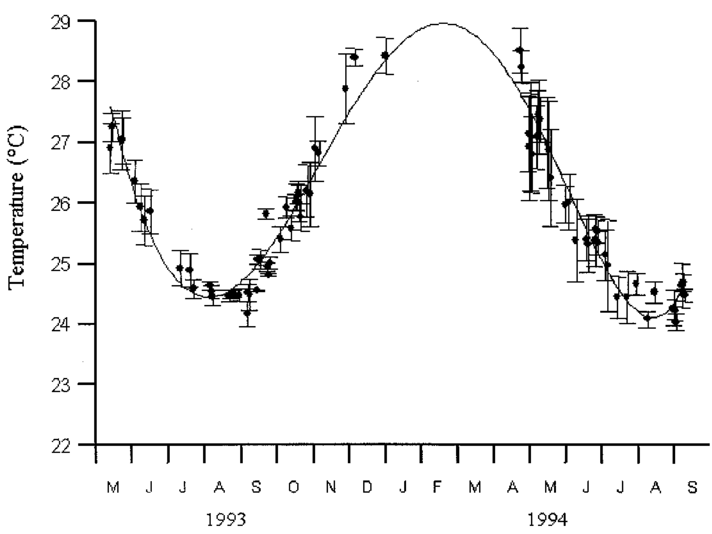

Figure 13. The mean ± 1 standard deviation of Lake Malawi surface temperature calculated from cloud-cleared AVHRR data taken between May 1993 and September 1994. Images with 10% cloud cover or less were used in this analysis.

indicate that the near-surface temperature estimates derived via remote sensing are representative of the bulk mixed epilimnetic layer, which represents the thermal barrier to lake water mixing. AVHRR-derived lake temperature maps are shown to portray information related to the 3-D thermal structure of the water, in particular on the horizontal and vertical displacement of lake isotherms and on large-scale upwelling events that are also observed via detailed *in situ* sampling. Analysis of 17 months of AVHRR data indicates that the mean surface (epilimnion) temperature most closely approaches that of the metalimnion in August, which is inferred to be the period of maximised mixing of these waters. During this period there will be increased nutrient loading from deeper waters into the trophogenic zone, with a corresponding increase in primary production. Ideally the use of AVHRR data for monitoring of lake surface temperatures into the future will continue to be supplemented by the input of *in situ* temperature measurements. These will be used to routinely check the continued validity of the AVHRR-based atmospheric correction algorithms and to prepare for further changes in operational satellite.

Acknowledgments

We thank the staff of the Lake Malawi Pelagic Fish Resource Assessment Project for their support and assistance with *in situ* and satellite data collection during this work. We also thank Dr Harvey Bootsma and colleagues of the GEF Lake Malawi/ Nyasa Biodiversity Conservation Project for continuing to support the study and for provision of *in situ* lake temperatures for 1997–98. We are grateful to Hanscom Airforce Base Geophysics Laboratory for provision of the MODTRAN code, to Roma Beaumont of King's College London for detailed redrawing of certain figures, and to Mr Danduala and Mr Kamdonyo of the Malawi Meteorological Department for supplying radiosonde and surface meteorological data for the year 1977. Dr Simon Brown of the UK Meteorological Office generously supplied additional radiosonde data for 1992. This work was funded by the UK Department for International Development (formally the Overseas Development Administration), and M Wooster is supported by the NERC Earth Observation Science Initiative.

References

Allison, E. H., Patterson, G., Irvine, K., Thompson, A. B., and Menz, A., 1995, The pelagic ecosystem. In *The Fishery Potential and Productivity of the Pelagic Zone of Lake Malawi/Niassa*, edited by A. Menz (Chatham: Natural Resources Institute), pp. 351–364.

Anding, D., and Kauth, R., 1970, Estimation of sea surface temperature from space. *Remote Sensing of Environment*, **1**, 217–220.

Barton, I., Zavody, A. M., O'Brien, D. M., Cutten, D. R., Saunders, R. W., and Llewellyn-Jones, D. T., 1989, Theoretical algorithms for satellite-derived sea surface temperatures. *Journal of Geophysical Research*, **94**, 3365–3375.

Berk, A., Bernstein, L. S., and Robertson, D. C., 1989, *MODTRAN: a moderate resolution model for LOWTRAN 7*, Technical Report PL-TR-89-0122, U.S. Air Force Phillips Laboratory, Hanscome Air Force Base, MA.

Brown, S., 1995, Satellite remote sensing of lake temperatures for climate research, Unpublished PhD thesis, University of London, London.

Byrnes, A. E., and Schott, J. R., 1986, Correction of thermal imagery for atmospheric effects using aircraft measurement and atmospheric modelling techniques. *Applied Optics*, **25**, 2563–2570.

Cracknell, A., 1997, *The Advanced Very High Resolution Radiometer* (London: Taylor and Francis).

Dengbol, P., and Mapila, S., 1982, Limnological studies of the pelagic zone of Lake Malawi from 1975–1981. In FAO MLW/75/019–Technical Report 1, UNFAO, Rome, pp. 3–48.

Eccles, D. H., 1974, An outline of the physical limnology of Lake Malawi (Lake Nyasa). *Limnology and Oceanography*, **19**, 730–742.

Hepplewhite, C. L., 1989, Remote observation of the sea surface and atmosphere, the oceanic skin effect. *International Journal of Remote Sensing*, **10**, 801–810.

Kidwell, K. B., 1995, *NOAA polar orbiter data users guide* (Washington DC: US Department of Commerce, National Oceanic and Atmospheric Administration).

Llewellyn-Jones, D. T., Minnet, P. J., Saunders, R. W., and Zavody, A. M., 1984, Satellite multichannel infrared measurements of sea surface temperature of the N.E. Atlantic Ocean using AVHRR/2. *Quarterly Journal of the Royal Meteorological Society*, **110**, 613–631.

Masuda, K., Takashima, T., and Takayama, Y., 1988, Emissivity of pure and sea waters for the model sea-surface in the infrared window regions. *Remote Sensing of Environment*, **24**, 313–329.

McLain, E. P., 1989, Global sea surface temperatures and cloud clearing for aerosol optical depth estimates. *International Journal of Remote Sensing*, **10**, 763–769.

McLain, E. P., Pichel, W. G., and Walton, C. C., 1985, Comparative performance of AVHRR based multi-channel sea surface temperatures. *Journal of Geophysical Research*, **86**, 11 587–11 601.

Menz, A., Bulirani, A., and Goodwin, C. M., 1995, Acoustic estimation of fish biomass. In *The Fishery Potential and Productivity of the Pelagic Zone of Lake Malawi/Niassa*, edited A. Menz (Chatham: Natural Resources Institute), pp. 307–349.

Patterson, G., and Kachinjika, O., 1995, Limnology and phytoplankton ecology. In *The Fishery Potential and Productivity of the Pelagic Zone of Lake Malawi/Niassa*, edited A. Menz (Chatham: Natural Resources Institute), pp. 1–67.

Patterson, G., Wooster, M. J., and Sear, C. B., 1995, *Real-time monitoring of African Aquatic Resources using Remote Sensing* (Chatham: Natural Resources Institute).

Saunders, R. W., and Kriebel, K. T., 1988, An improved method for detecting clear sky and cloudy radiances from AVHRR data. *International Journal of Remote Sensing*, **9**, 123–150.

Talling, J., and Lemoalle, J., 1998, *Ecological Dynamics of Tropical Inland Waters* (Cambridge: Cambridge University Press).

Walton, A. E., 1985, Satellite measurement of sea surface temperature in the presence of volcanic aerosols. *Journal of Climate and Applied Climatology*, **24**, 501–507.

Wooster, M. J., Sear, C. B., and Patterson, G., 1994a, Tropical lake surface temperatures from locally received NOAA-11 AVHRR data—comparison with *in situ* measurements. *International Journal of Remote Sensing*, **15**, 183–189.

Wooster, M. J., Sear, C. B., and Patterson, G., 1994b, The use of a PC-based AVHRR receiving station for mapping tropical lake surface temperature. In *Proceedings of the Second Thematic Conference on Remote Sensing for Marine and Coastal Environments* (New Orleans: ERIM), January 1994, pp. 431–441.

Wooster, M. J., Richards, T., and Kidwell, K. B., 1995, NOAA-11 AVHRR/2—thermal channel calibration update. *International Journal of Remote Sensing*, **16**, 359–363.